Structural features of human inositol phosphate multikinase rationalize its inositol phosphate kinase and phosphoinositide 3-kinase activities

Received for publication, June 14, 2017, and in revised form, September 1, 2017 Published, Papers in Press, September 7, 2017, DOI 10.1074/jbc.M117.801845

Huanchen Wang[1] **and Stephen B. Shears**

From the Inositol Signaling Group, Signal Transduction Laboratory, NIEHS, National Institutes of Health, Research Triangle Park, North Carolina 27709

Edited by Joseph Jez

Human inositol phosphate multikinase (*Hs*IPMK) critically contributes to intracellular signaling through its inositol-1,4,5-trisphosphate (Ins(1,4,5)P_3) 3-kinase and phosphatidylinositol 4,5-bisphosphate (PtdIns(4,5)P_2) 3-kinase activities. This catalytic profile is not conserved; orthologs from *Arabidopsis thaliana* and *Saccharomyces cerevisiae* are predominantly Ins(1,4,5)P_3 6-kinases, and the plant enzyme cannot phosphorylate PtdIns(4,5)P_2. Therefore, crystallographic analysis of the yeast and plant enzymes, without bound inositol phosphates, do not structurally rationalize *Hs*IPMK activities. Here, we present 1.6-Å resolution crystal structures of *Hs*IPMK in complex with either Ins(1,4,5)P_3 or PtdIns(4,5)P_2. The Ins(1,4,5)P_3 headgroup of PtdIns(4,5)P_2 binds in precisely the same orientation as free Ins(1,4,5)P_3 itself, indicative of evolutionary optimization of 3-kinase activities against both substrates. We report on nucleotide binding between the separate N- and C-lobes of *Hs*IPMK. The N-lobe exhibits a remarkable degree of conservation with protein kinase A (root mean square deviation = 1.8 Å), indicating common ancestry. We also describe structural features unique to *Hs*IPMK. First, we observed a constrained, horseshoe-shaped substrate pocket, formed from an α-helix, a 3_{10} helix, and a recently evolved tri-proline loop. We further found *Hs*IPMK activities rely on a preponderance of Gln residues, in contrast to the larger Lys and Arg residues in yeast and plant orthologs. These conclusions are supported by analyzing 14 single-site *Hs*IPMK mutants, some of which differentially affect 3-kinase and 6-kinase activities. Overall, we structurally rationalize phosphorylation of Ins(1,4,5)P_3 and PtdIns(4,5)P_2 by *Hs*IPMK.

Considerable attention is focused on the enzymes that regulate the metabolism and hence the myriad cell signaling activities of the inositol phosphates and the inositol lipids. These are two physicochemically and functionally distinct groups of intracellular signals (1), which typically each rely on separate families of kinases for their synthesis. The sole exception is the inositol phosphate multikinase, initially named for its ability to phosphorylate inositol phosphates (2, 3), but later found to also phosphorylate PtdIns(4,5)P_2 (4). This "dual-specificity" has endowed the inositol phosphate multikinase (IPMK)[2] family with multiple biological activities. For example, IPMK is indispensable for connecting PLC-mediated Ins(1,4,5)P_3 release to the generation of InsP_5 (5–7); the latter is a precursor for InsP_6 and the inositol pyrophosphates, which each have many cellular functions (1, 8). Activation of the inositol phosphate kinase activities of IMPK appears to be a key response in the Wnt/β-catenin signaling pathway (9). IPMK is mainly localized in the nucleus (4, 10, 11), where its kinase activities have been shown to mediate cellular differentiation programs (12), and transcript-selective mRNA export from the nucleus (13). Also in the nucleus, the PtdIns(4,5)P_2 3-kinase activity of IPMK stimulates the transcriptional activity of the nuclear receptor steroidogenic factor 1 (14). In addition, mammalian IPMK has moonlighting functions, unrelated to its catalytic activities, which are mediated through interactions with a number of protein-binding partners, such as mTOR (mechanistic target of rapamycin) (15), p53 (16), and AMP-activated protein kinase (17).

The wide-ranging importance of the IPMKs is underscored by the observation that knock-out of the *IPMK* gene in mice is embryonic lethal (5). There are also some pathological consequences for genetic defects in human *IPMK* that have been associated with a reduction in its kinase activities. For example, a heterozygous, frameshift mutation in the human *IPMK* gene has been identified in six members of the same family who all developed small intestinal neuroendocrine tumors; these individuals also exhibited a reduction in InsP_5 synthesis (18). Additionally, impaired *IPMK* transcription and a decrease in IPMK stability has been linked to the pathology of Huntington's disease, by virtue of an attenuation of the PtdIns(3,4,5)P_3/AKT

This work was supported by the Intramural Research Program of the National Institutes of Health, NIEHS. The authors declare that they have no conflicts of interest with the contents of this article. The content is solely the responsibility of the authors and does not necessarily represent the official views of the National Institutes of Health.

The atomic coordinates and structure factors (codes 5W2G, 5W2H, and 5W2I) have been deposited in the Protein Data Bank (http://wwpdb.org/).

[1] To whom correspondence should be addressed: 111 T.W. Alexander Dr., Research Triangle Park, NC 27709. Tel.: 919-541-0793; E-mail: wangh7@niehs.nih.gov.

[2] The abbreviations used are: IPMK, inositol phosphate multikinase; AMP-PNP, adenylyl-imidodiphosphate; Ins(1,4,5)P_3, inositol-1,4,5-trisphosphate; Ins(1,3,4,5)P_4, inositol-1,3,4,5-tetrakisphosphate; Ins(1,4,5,6)P_4, inositol-1,4,5,6-tetrakisphosphate; Ins(1,3,4,5,6)P_5, inositol-1,3,4,5,6-pentakisphosphate; IP3K, inositol-1,4,5-trisphosphate 3-kinase; IP6K, inositol hexakisphosphate kinase; PIK3CA, PtdIns(4,5)P_2 3-kinase 110-kDa catalytic subunit α; PtdIns(4,5)P_2, phosphatidylinositol 4,5-bisphosphate; PtdIns(3,4,5)P_3, phosphatidylinositol 3,4,5-trisphosphate; GroPtdIns(4,5)P_2, glycerophosphoinositol 4,5-bisphosphate; r.m.s. deviation, root mean square deviation; PDB, Protein Data Bank.

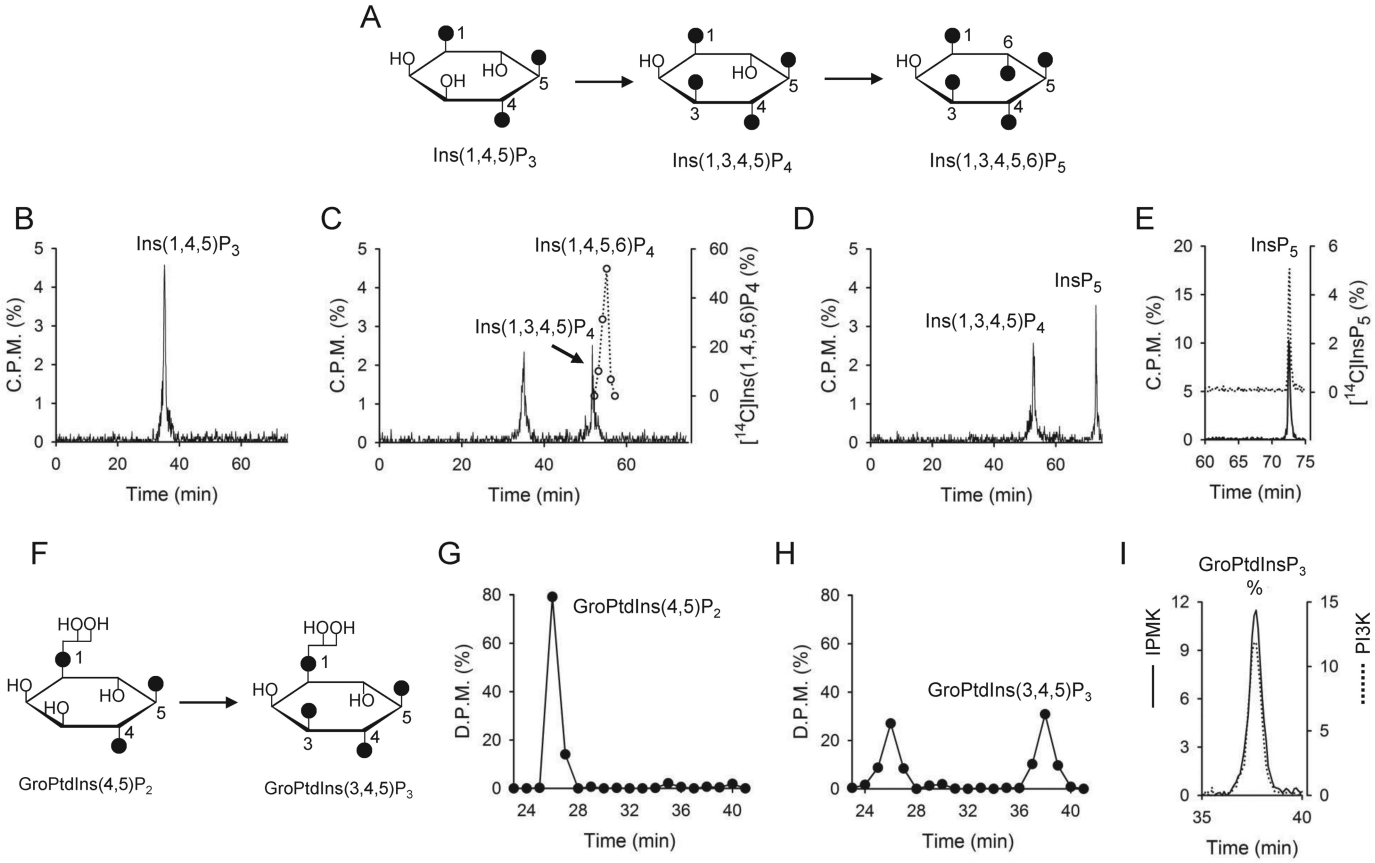

Figure 1. The inositol phosphate and inositol lipid kinase activities of *HsIPMK*. *A*, graphic depicting the successive Ins(1,4,5)P_3 3-kinase and Ins(1,3,4,5)P_4 6-kinase activities of *Hs*IPMK; *filled circles* represent phosphate groups. *B*, HPLC analysis of [^{3}H]Ins(1,4,5)P_3 at zero time (*solid line*). *C*, HPLC analysis of the phosphorylation of [^{3}H]Ins(1,4,5)P_3 for 15 min by 0.9 ng *Hs*IPMK (*solid line*). Also shown is the elution of a [^{14}C]Ins(1,4,5,6)P_4 standard (*open circles*; *dotted line*) obtained in parallel to a run by collecting fractions. *D*, HPLC analysis of the phosphorylation of [^{3}H]Ins(1,4,5)P_3 for 15 min by 90 ng of *Hs*IPMK (*solid line*). *E*, the elution of a [^{14}C]Ins(1,3,4,5,6)P_5 standard (*dotted line*) obtained in parallel to an assay in which [^{3}H]Ins(1,4,5)P_3 was phosphorylated to [^{3}H]Ins(1,3,4,5,6)P_5 by *Hs*IPMK (*solid line*). *F*, graphic depicting GroPtd[^{3}H]Ins(4,5)P_2 3-kinase activity of *Hs*IPMK. *G*, HPLC analysis of GroPtd[^{3}H]Ins(4,5)P_2 at zero time. *H*, HPLC analysis of phosphorylation of GroPtd[^{3}H]Ins(4,5)P_2 to GroPtd[^{3}H]InsP_3 (elution peak = 38 min) by 4.5 ng of *Hs*IPMK for 15 min. *I*, *Hs*IPMK (9.5 ng) was incubated for 16 h with [^{32}P]ATP and diC$_8$-PtdIns(4,5)P_2; the diC$_8$-Ptd[^{32}P]Ins(3,4,5)P_3 product was deacylated to GroPtd[^{32}P]InsP_3, which was analyzed by HPLC (*solid line*). In a parallel HPLC run, we analyzed a GroPtd[^{32}P]InsP_3 standard (*dotted line*), derived from PtdIns(4,5)P_2 3-kinase 110-kDa catalytic subunit α (PIK3CA). The elution peak = 37.7 min. Full details are provided under "Experimental procedures."

signaling cascade (19). Genome-wide association studies have described that decreased IPMK expression in brain tissue is associated with the pathogenesis of inflammation-associated neurodegeneration (20).

IPMK is a member of the so-called IP-kinase family that includes IP3Ks and IP6Ks (21). Characterization of the structures of each of these enzymes can rationalize their alternate catalytic specificities, assist in deciphering evolutionary relationships, and permits rational design of enzyme-specific inhibitors. Previous work has described crystal structures of an IP3K (21, 22) and an IP6K (23), each with substrates captured in the active site. Two previous studies have described the crystal structures of IPMK orthologues from *Saccaromyces cerevisiae* (24) and *Arabidopsis thaliana* (25), at resolutions of 2 and 2.9 Å, respectively. However, neither study captured inositol phosphate within the active site.

Molecular modeling has generated a consensus view that IPMKs host a relatively spacious and conformationally flexible substrate-binding pocket, in which mobile side chains of Lys and Arg residues play major roles (24, 25). Here, we demonstrate that this model does not apply to *Hs*IPMK; we describe a catalytic pocket that is more constrained than those of the plant and yeast orthologs. Also unique to mammalian IPMK is a catalytically important proline-loop, and a preponderance of Gln residues in the active site. These conclusions are drawn from our description, for the first time, of the crystal structure of *Hs*IPMK. Moreover, we present the first structures of *any* IPMK in complex with inositol phosphate substrate: we describe two versions of Ins(1,4,5)P_3 within the active site, first as a free inositol phosphate, and second as the headgroup of a soluble analogue of PtdIns(4,5)P_2. This allows a structural rationalization of 3-kinase activity toward Ins(1,4,5)P_3 and PtdIns(4,5)P_2.

Results and discussion

General structure of HsIPMK

Previous work (3, 4, 11, 14) has shown that *Hs*IPMK is both an inositol phosphate kinase and a PtdIns(4,5)P_2 kinase. Here, we confirmed that recombinant *Hs*IMPK uses 3-kinase activity to phosphorylate Ins(1,4,5)P_3 to Ins(1,3,4,5)P_4, and then phosphorylates the latter with a 6-kinase activity that yields Ins(1,3,4,5,6)P_5 (Fig. 1, *A*–*E*). In addition, we used a deacylated, soluble version of Ptd[^{3}H]InsP(4,5)P_2 (*i.e.* GroPtd[^{3}H]Ins

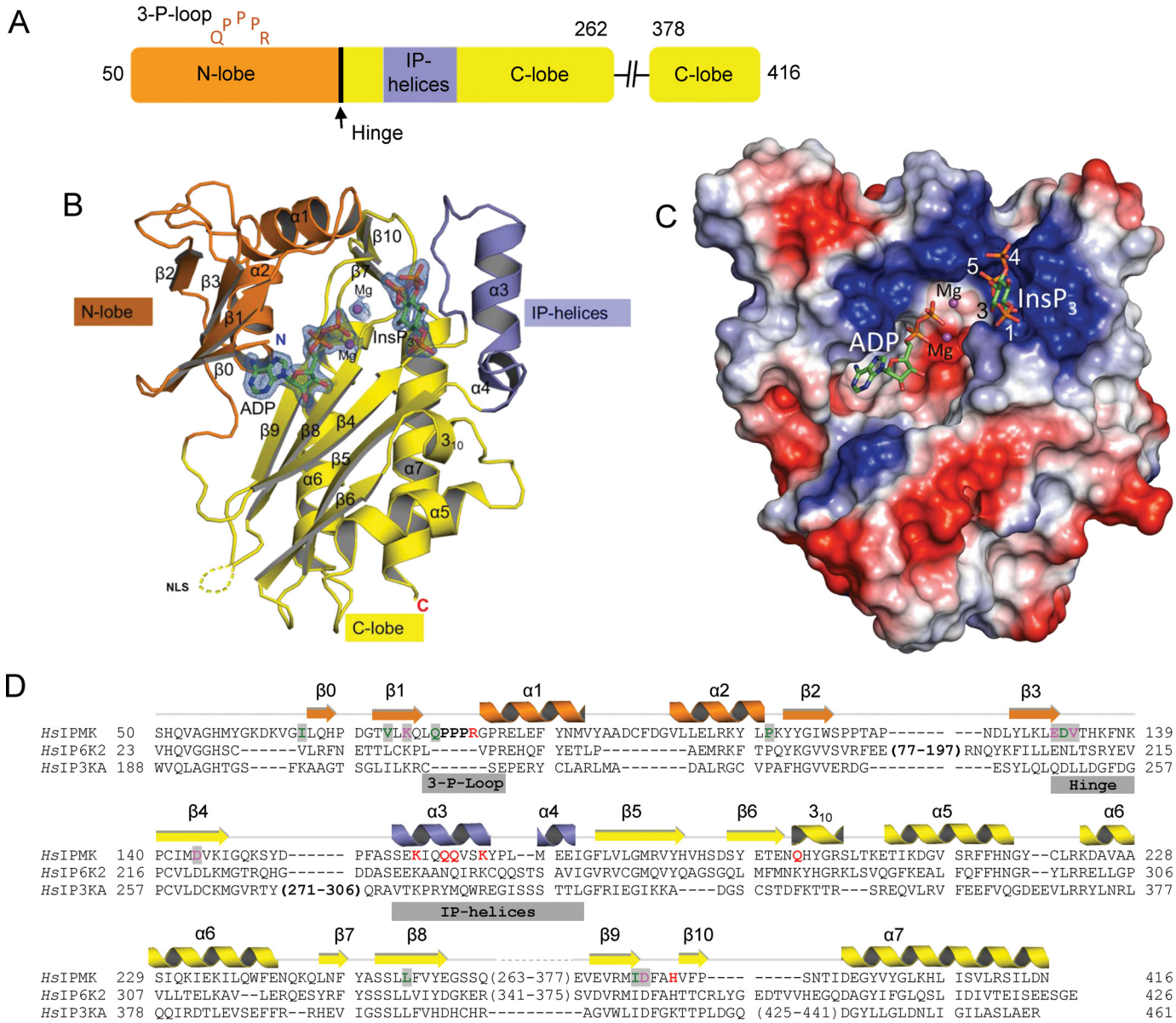

Figure 2. Overall structure of the ADP-Ins(1,4,5)P_3-*HsIPMK* crystal complex. *A*, domain graphic of the *Hs*IPMK construct used for structural characterization, based on previously published terminology (21). Note that amino acid residues in a domain responsible for nuclear localization (263 to 377) were replaced with a Gly-Gly-Ser-Gly-Gly linker. *B*, ribbon plot of the *Hs*IPMK structure. *NLS* = nuclear localization sequence. ADP and $InsP_3$ are shown as stick models within an $2F_o - F_c$ electron density, which is contoured at 1.5 σ. Two magnesium atoms are depicted as *magenta balls*. *C*, electrostatic surface plot with *blue* and *red* coloration to denote positive and negative electrostatic potentials, respectively, at physiological pH. *D*, a manual alignment of amino acid sequences (*Hs*IPMK, NP_689416.1; *Hs*IP6K2, NP_057375.2; and *Hs*IP3KA, NP_002211.1), guided by the structural elements that have been observed in crystal structures, and in the case of *Hs*IP6K2, secondary structural predictions. The secondary structural elements from *HsIPMK* are depicted *above* its sequence and are color-coded *orange* for the N-lobe, *yellow* for the C-lobe, and *blue* for the IP-helices. Residues are involved in ATP binding are highlighted as *magenta* for polar contacts and *green* for Van der Waals interactions. Residues that are involved in Ins(1,4,5)P_3 binding are highlighted in *red*. The loop that contains three prolines ("3-P"), and the hinge between the N- and C-domains, are also highlighted. PDB codes for *HsIPMK* are 5W2G, 5W2H, and 5W2I.

(4,5)P_2) to confirm the PtdIns(4,5)P_2 3-kinase activity of recombinant *Hs*IPMK (Fig. 1, *F–I*). Our next goal was to rationalize these various kinase reactions structurally, at an atomic level.

We produced crystals of the core catalytic domain of the enzyme that contains residues 50 to 416, from which we deleted an internal domain comprising residues 263 to 377 (Fig. 2*A*); that deletion, which was necessary to obtain crystals, was replaced with a simple Gly-Gly-Ser-Gly-Gly linker (Fig. 2*A*). Previous work has shown that this deletion does not compromise catalytic activity (26); this is a non-catalytic region of the protein. It contains a nuclear localization sequence, flanked by residues that host protein kinase phosphorylation sites that regulate nuclear localization sequence functionality (26).

The structure of the IPMK apoenzyme was determined by a molecular replacement approach using a model constructed from the template of *Sc*IPMK (PDB accession code 2IF8). That information was then used for further elucidation of the structures of crystal complexes with ADP plus either Ins(1,4,5)P_3 (Fig. 2, *A–D*) or diC$_4$-PtdIns(4,5)P_2 (see below).

For each asymmetric unit, there is one molecule of IPMK in space group $P4_22_12$ (Table 1). Analysis of the overall fold of *Hs*IPMK (Fig. 2*B*) reveals domains that are similar to the so-

Table 1
Data collection and structure refinement statistics

PDB accession IDs	5W2G	5W2H	5W2I
Ligand	Apo	ADP-Ins (1,4,5) P_3-Mg	ADP-DiC4-PtdInsP_2-Mg
Data collection			
Space group	$P4_22_12$	$P4_22_12$	$P4_22_12$
Cell dimensions *a, c* (Å)	78.47, 85.65	78.02, 85.92	78.09, 86.32
Resolution (Å)[a]	50–1.80 (1.83)	50–1.9 (1.93)	50–1.6 (1.63)
R_{meas}[a]	0.121 (0.857)	0.116 (0.953)	0.104 (0.782)
CC1/2 in the highest shell	0.754	0.763	0.853
$I/\sigma I$[a]	15.5 (3.6)	18.0 (3.3)	22.1 (2.9)
Completeness (%)[a]	99.4 (99.9)	99.9 (100.0)	99.9 (100.0)
Redundancy[a]	8.7 (8.1)	9.0 (8.9)	7.7 (7.3)
Refinement			
Resolution(Å)[a]	1.80 (1.85)	1.9 (1.95)	1.6 (1.64)
No. reflections	23558	20189	34007
R_{work}[a]	17.1 (24.6)	16.3 (19.1)	16.9 (18.7)
R_{free}[a]	21.5 (25.7)	23.0 (30.2)	21.5 (23.7)
No. atoms			
Protein	2034	2046	2035
Mg		2	2
Inositol phosphates		24	24
ADP		27	27
Solvent	154	177	182
B-factors (Å^2)			
Protein	25.1	24.7	17.8
Mg		17.4	15.6
Inositol phosphates		34.5	25.2
ADP		17.6	13.7
Solvent	35.2	36.4	33.7
R.m.s. deviations			
Bond length(Å)	0.008	0.010	0.009
Bond angle (°)	1.285	1.54	1.39

[a] The numbers in parentheses are for the highest resolution shell.

called N- and C-lobes that comprise the ATP-binding sites in the orthologs *Sc*IPMK (24) and *At*IPMK (25), as well as *Eh*IP6KA (23) and *Hs*IP3KA (21). Superimposition structures of each of these proteins with *Hs*IPMK reveals root mean square deviations (r.m.s. deviations) of 0.93 Å for *Sc*IPMK (139 comparable Cα atoms), 1.37 Å for *At*IPMK (149 comparable Cα atoms), 1.65 Å for *Eh*IP6KA (145 comparable Cα atoms), and 1.14 Å for *Hs*IP3KA (144 comparable Cα atoms).

The N-terminal lobe in *Hs*IPM*K* is designated by residues 65–135, which consist of four antiparallel β-strands and two short helices α1 and α2 and the β1 and β3 strands. Residues 66–69 lie within a β-strand that has not been observed in either *Sc*IPMK or *At*IPMK; we designated this the β0 strand. We designated the C-terminal lobe as comprising residues 136–149 and 175–416, which is an $\alpha+\beta$-fold with five, central antiparallel β-strands including β4–6, β8, and β9, a pair of small antiparallel β-strands (β7 and β10), and three α–helices (α5-α7). Also in the C-lobe of *Hs*IPMK, a 3_{10} helix was observed between the β6 strand and α5 helix. An equivalent, albeit longer 3_{10} helix is present in *Eh*IP6KA, where it is important for substrate binding (23).

Description of the nucleotide-binding region of HsIPMK

We soaked Ins(1,4,5)P_3, ATP, and magnesium into the apoenzyme crystals. Nucleotide binding did not alter protein conformation. The ADP moiety was observed (Fig. 3*A*), but not the γ-phosphate of ATP. A similar result was obtained in an earlier study with *Sc*IPMK (24). Perhaps in our study, the γ-phosphate was hydrolyzed, or alternately, disordered in the crystal. The latter explanation is feasible, because the terminal phosphate of adenylyl-imidodiphosphate (AMP-PNP) was also the only portion of that non-hydrolyzable ATP analogue that we could not visualize, after it was soaked into the crystal structure with Ins(1,4,5)P_3.[3]

*Hs*IPMK clasps the nucleotide between the N- and C-lobes, which are linked by a hinge that comprises residues Asp^{132} to Pro^{140} (Figs. 2, *A* and *C*, and 3*A*). The N^1 and N^6 atoms of adenine both make hydrogen bonds with the polypeptide backbone: N^1 contacts the amide nitrogen of Val^{133} from the hinge, and N^6 interacts with the carbonyl oxygen of Glu^{131} from the N-lobe (Fig. 3*A*). The ATP-ribose group is loosely confined by several van der Waals contacts with Leu^{254} and Ile^{384}, plus one hydrogen bond with Asp^{144}. The α-phosphate of the nucleotide forms a salt bridge with Lys^{75} (Fig. 3*A*). Asp^{385} interacts with two magnesium ions to make contact with the α- and β-phosphates of ADP. The particular importance of Asp^{385} is reflected in it being part of an Ile-Asp-Phe tripeptide that is conserved throughout the IP-kinase family (Figs. 2*D* and 3*A*, and see Ref. 21).

Key residues in the nucleotide-binding pocket of *Hs*IPMK were superimposed upon those of *Sc*IPMK, revealing a high degree of conservation (Fig. 3*B*; the same comparison could not be made with *At*IPMK, because no nucleotide-bound crystal structures are available). Moreover, data in Fig. 3*C* show that five of the residues in *Hs*IPMK that make contacts with ADP, namely, Lys^{75}, Glu^{131}, Val^{133}, Asp^{144}, and Asp^{385}, are also represented in the nucleotide-binding domain of protein kinase A (PKA) (27). Furthermore, a high degree of conservation of the entire N-lobes was revealed by superimposition of the secondary structure elements of the *Hs*IPMK structure upon those in PKA (Fig. 3*D*): a core r.m.s. deviation of 1.80 Å (51/69 comparable residues). The C-lobes (Fig. 3*E*) are less conserved: a core r.m.s. deviation of 3.35 Å (78/168 comparable residues). The major structural differences between the C-lobes of the two proteins reflects specialization of the alternative substrate-binding pockets. The C-lobe of PKA, and indeed protein kinases in general, contains a greater degree of helical structure, and a wider binding site to accommodate a polypeptide (27, 28) (Fig. 3*F*). These data confirm and extend the idea (21, 29) that protein kinases and the so-called IP-kinase family share an evolutionary ancestry.

Description of inositol phosphate binding

The successful soaking of Ins(1,4,5)P_3 into *Hs*IPMK crystals (Fig. 2, *B* and *C*) has yielded the first description of any inositol phosphate substrate captured in the active site of an IPMK. Simulated annealing omit maps and $2F_o - F_c$ maps clearly identify the inositol ring and individual phosphate groups for Ins(1,4,5)P_3 (Fig. 2*B*). The 2–5 axis of the Ins(1,4,5)P_3 substrate inserts vertically into a positively charged (at physiological pH) horseshoe-shaped pocket (Fig. 4*A*) constructed from (in anticlockwise rotation), a short 3_{10} helix, the α3 helix, and a unique loop that is fabricated from three proline residues (Fig. 4*B*). Rigidity in the α3 helix is enhanced by virtue of a 2.8-Å hydrogen bond between the carboxyl and amine groups in the side chains of Gln^{163} and Gln^{164}, respectively (Fig. 5*A*). This constrains the conformations of the two side chains and introduces

[3] H. Wang, unpublished data.

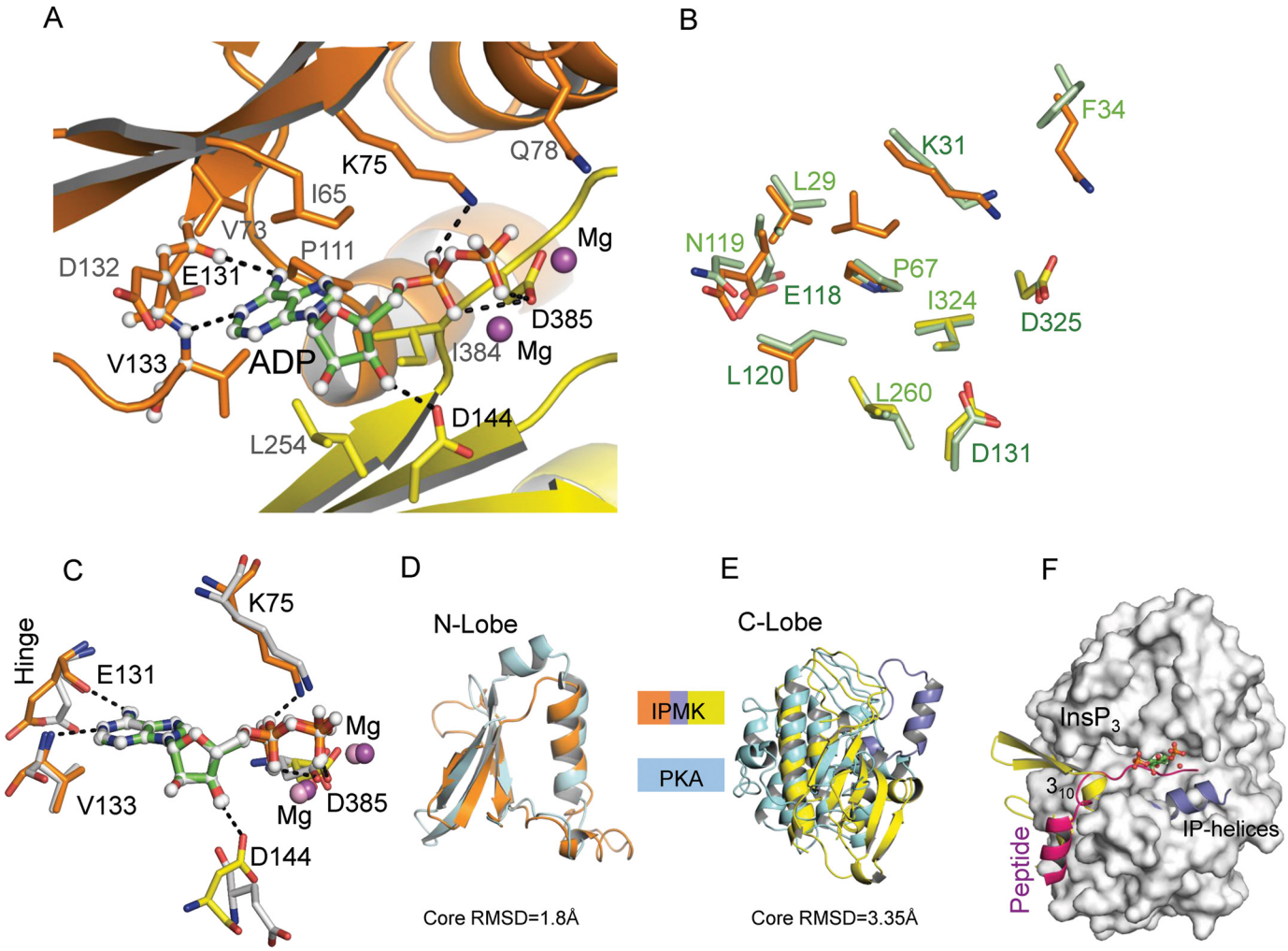

Figure 3. Nucleotide binding by *Hs*IMPK; conservation of a microenvironment in *Hs*IPMK and protein kinase A. *A*, ADP is depicted as a stick and ball model. The *HsIPMK*-bound ADP are show in *green* for carbon, *red* for oxygen, *blue* for nitrogen, and *orange* for phosphorus atoms. Two magnesium atoms are depicted as *magenta spheres*. Polar contacts are shown with *dashed lines*. Amino acids side chains are shown as *sticks*. The backbones of the hinge residues are also shown as stick and ball models. *B*, superimposition of key residues for nucleotide binding between *Hs*IPMK (*orange* or *yellow stick*, residues are numbered as in *panel A*) and *Sc*IPMK (*light green stick*, with *green*-colored residues numbers). *C*, shows conservation of both the nature and the relative positions of the nucleotide-binding residues in *Hs*IPMK (*orange*, *blue*, and *yellow sticks*) and PKA from the rat (*white sticks*; PDB code 1L3R). PKA-bound nucleotide is depicted in *white*. The magnesium atoms in *Hs*IPMK are shown in *magenta*; those from PKA are colored *pink*. *D–F*, superimpositions of *Hs*IPMK and PKA. *D* and *E* are ribbon plots of the N- and C-lobe, respectively, of *Hs*IPMK (*orange*, *blue*, and *yellow*) and PKA (*cyan*). *F*, a surface representation of PKA (*white*) in complex with the peptide substrate; Ins(1,4,5)P_3 (*green* carbon stick and ball), from the HsIPMK structure (*yellow* and *blue* schematics), is located in the PKA catalytic center.

planarity, resulting in a stacking effect between the inositol ring and the α3 helix.

The proline loop of *Hs*IPMK (Fig. 4*B*) is a structural element that is absent from *Hs*IP3K (Figs. 2*D* and 4*C*) and both the plant and yeast IPMKs (Fig. 4, *D* and *E*, and 5*B*). In fact, in our IPMK sequence alignment (Fig. 5*B*), there are gaps in the yeast and plant sequences in the region corresponding to the *Hs*IPMK proline loop. Interestingly, the equivalent *Drosophila* IPMK sequence is Lys-Pro-Glu, suggesting that a nascent version of this loop is present in this, and perhaps, other invertebrates (Fig. 5*B*). Arg^{82} at the N terminus of the proline-loop makes 3 polar contacts with the 4- and 5-phosphates of Ins(1,4,5)P_3, indicating its particular importance in substrate binding. Gln^{78}, at the N terminus of the proline loop, interacts with two water molecules that coordinate with the β-phosphate of ADP and a magnesium atom (Fig. 4*B*).

We were unable to visualize the γ-phosphate of ATP within the catalytic center, apparently because it is disordered in the crystal (see above), but the ADP moiety is only 6.3 Å from the 3-OH of Ins(1,4,5)P_3 that is phosphorylated (Fig. 5, *A* and *C*). Thus, ATP may phosphorylate the Ins(1,4,5)P_3 substrate by direct, in-line transfer (Fig. 5*C*). There are also two magnesium ions that are in a position to stabilize the negative charge that would develop on the leaving γ-phosphoryl group. Additionally, His^{388} is also only 7.7 Å from the β-phosphate of the ADP moiety, and so it is possible that His^{388} may contribute to charge balance during catalysis. His^{388} can also hydrogen bond with the 4-phosphate of Ins(1,4,5)P_3 (Fig. 5*A*).

Other residues that form polar contacts with Ins(1,4,5)P_3 include Lys^{160}, Gln^{163}, Gln^{164}, and Lys^{167} from the α3 helix, and Gln^{196} from the 3_{10} helix (Fig. 5*A*). A contact between Gln^{164} and the axial 2-hydroxyl group appears to help locate the inositol ring near-parallel to the α3 helix (Figs. 4*A* and 5*A*). The interactions of Gln^{164}, Lys^{167}, and Gln^{196} with Ins(1,4,5)P_3 may be particularly important for enforcing its phosphorylation at the 3-position. Thus, we have described a relatively constrained

Table 2

Effects upon the catalytic activities of *Hs*IPMK following mutation of key residues to Ala

Rate equations (see under "Experimental procedures") were used to derive the individual first-order rate constants k_1, k_2, and k_3. Data are mean ± S.E. from 3 to 6 determinations.

Mutant	Location	k_1 (s^{-1}) $InsP_3$ metabolism (3-kinase)	Δ	k_2 (s^{-1}) $InsP_5$ synthesis (6-kinase)	Δ	k_3 (s^{-1}) $GroPIns(4,5)P_2$ metabolism (3-kinase)	Δ
			-fold		*-fold*		*-fold*
None (WT)		56.1 ± 2.0		0.64 ± 0.02		11.3 ± 0.2	
Q78A	Proline-loop	5.4 ± 0.6	−10	0.17 ± 0.03	−4	ND[a]	
R82A	Proline-loop	1.6 ± 1.0	−35	0.01 ± 0.0005	−64	ND	
K160A	IP-helix	0.8 ± 0.08	−67	0.01 ± 0.001	−64	ND	
Q163A	IP-helix	20.6 ± 1.65	−3	0.36 ± 0.011	−2	ND	
Q164A	IP-helix	0.5 ± 0.04	−119	0.006 ± 0.0003	−107	0.08 ± 0.002	−141
K167A	IP-helix	7.0 ± 0.56	−8	0.091 ± 0.004	−7	6.7 ± 0.4	−2
Q196A	3_{10} helix	14.0 ± 1.4	−4	0.22 ± 0.012	−3	6.5 ± 0.4	−2
H388A	Catalytic center	0.1 ± 0.004	−584	0.00031 ± 0.00006	−206	ND	

[a] ND, not determined.

Table 3

Differential effects of mutagenesis of catalytically-important Gln residues upon 3-kinase and 6-kinase activities of IPMK

Data are mean ± S.E. from 3 to 6 determinations. There was no significant accumulation of $Ins(1,4,5,6)P_4$ in these experiments.

Mutant	k_1 (s^{-1}) $InsP_3$ metabolism	Δ	k_2 (s^{-1}) $InsP_5$ synthesis	Δ	k_1/k_2
		-fold		-fold	
None (WT)	56.1		0.64		88
Q163K	6.3 ± 0.4	−9	0.41 ± 0.04	−2	16
Q163R	9.3 ± 0.9	−6	0.68 ± 0.02	0	14
Q164K	3.1 ± 0.2	−18	0.31 ± 0.05	−2	10
Q164R	8.3 ± 0.8	−7	8.5 ± 1.06	13	1
Q196K	19.4 ± 1.1	−3	2.4 ± 0.1	4	8
Q196R	12.3 ± 1.4	−4.5	3.1 ± 0.4	5	4

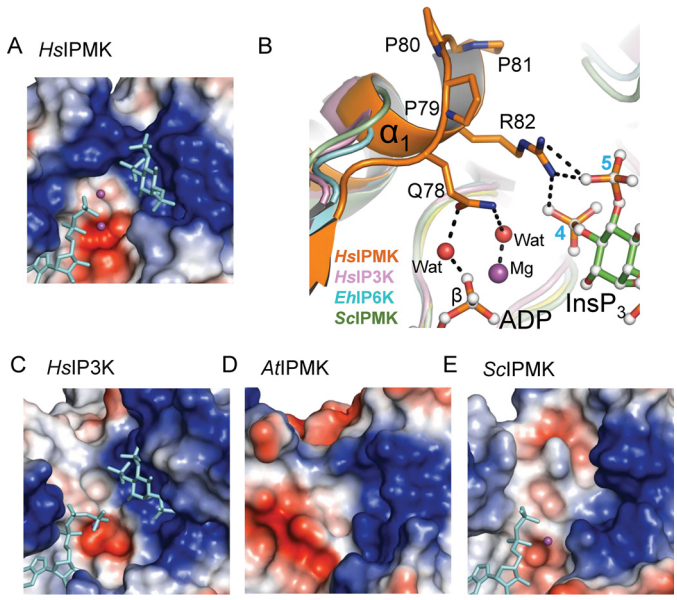

Figure 4. The proline loop of *Hs*IPMK. *A*, electrostatic surface plot of the catalytic site of *Hs*IPMK. $Ins(1,4,5)P_3$ and ADP are depicted as *cyan sticks*. Magnesium atoms are shown in *magenta*. *B*, the proline loop that is unique to *Hs*IPMK (*orange schematic*) is shown in a structural superimposition of that protein with *Hs*IP3K (*pink*, PDB code 1W2C), *Entamoeba histolytica* IP6K (*cyan*, PDB code 4O4F), and *Sc*IPMK (*green*, PDB code 2IF8). ADP and $Ins(1,4,5)P_3$ are shown in stick and ball models (*green stick* for carbon, *red* for oxygen, and *orange* for phosphorus atoms). *C*, electrostatic surface plot of the catalytic site of *Hs*IP3K; $Ins(1,4,5)P_3$ and ADP are shown in *cyan sticks*. *D* and *E*, electrostatic surface plots of the catalytic sites of *At*IPMK and *Sc*IPMK, respectively. These crystal complexes do not contain an inositol phosphate in the active site. ADP is shown in *cyan sticks*.

catalytic pocket in which a preponderance of Gln residues make contact with substrate. This contrasts with the description of the active site that emerged from the modeling of substrates into the active sites of *At*IPMK (25) and *Sc*IPMK (24). The latter two studies described a less-enclosed and conformationally-flexible substrate pocket in which mobile side chains of Lys and Arg residues play major roles in ligand binding (Fig. 5, *D* and *E*). Two such residues in particular, Lys^{153} and Arg^{156} in *At*IPMK, were proposed to form key contacts with substrate (25). In a structural alignment (Fig. 5*E*), the latter two residues correspond to His^{197} and Arg^{200} in HsIPMK (Fig. 5*E*), but these do not play any role in substrate-binding in our crystal structures (Fig. 5, *A* and *E*).

As noted above, *Hs*IPMK phosphorylates $Ins(1,4,5)P_3$ to $Ins(1,3,4,5)P_4$ and then to $Ins(1,3,4,5,6)P_5$. We were unsuccessful in our efforts to soak $Ins(1,3,4,5)P_4$ into the crystals, so we modeled this particular substrate into the active site (Fig. 6, *A* and *B*). We found we could accomplish this, such that the 6-OH of $Ins(1,3,4,5)P_4$ is the group closest to the active site, by a 180° flip of the 3–6 axis of the inositol ring of $Ins(1,3,4,5)P_4$, relative to that of $Ins(1,4,5)P_3$ (Fig. 6, *A* and *B*). We therefore conclude that *Hs*IMPK is unlikely to processively phosphorylate $Ins(1,4,5)P_3$ to $Ins(1,3,4,5,6)P_5$; instead, it appears that the $Ins(1,3,4,5)P_4$ intermediate must dissociate and rebind in a different orientation.

In our model (Fig. 6*B*), the 4- and 5-phosphates of $Ins(1,3,4,5)P_4$ spatially mimic the orientation of the 5- and 4-phosphates of $Ins(1,4,5)P_3$, respectively. This model (Fig. 6) further predicts that the 3-phosphate of $Ins(1,3,4,5)P_4$ could gain up to two polar contacts with Gln^{163} and Lys^{167}. Nevertheless, the overall conclusion is that, compared with $Ins(1,4,5)P_3$, the $Ins(1,3,4,5)P_4$ makes fewer total interactions with the protein. For example, the 1-phosphate of $Ins(1,3,4,5)P_4$ only makes 2 contacts with Lys^{167} and Gln^{196}, whereas the 1-phosphate of $Ins(1,4,5)P_3$ makes 4 contacts with the same two residues. Second, Gln^{164} interacts with $Ins(1,4,5)P_3$ at the axial 2-OH, but this group in $Ins(1,3,4,5)P_4$ does not directly interact with the

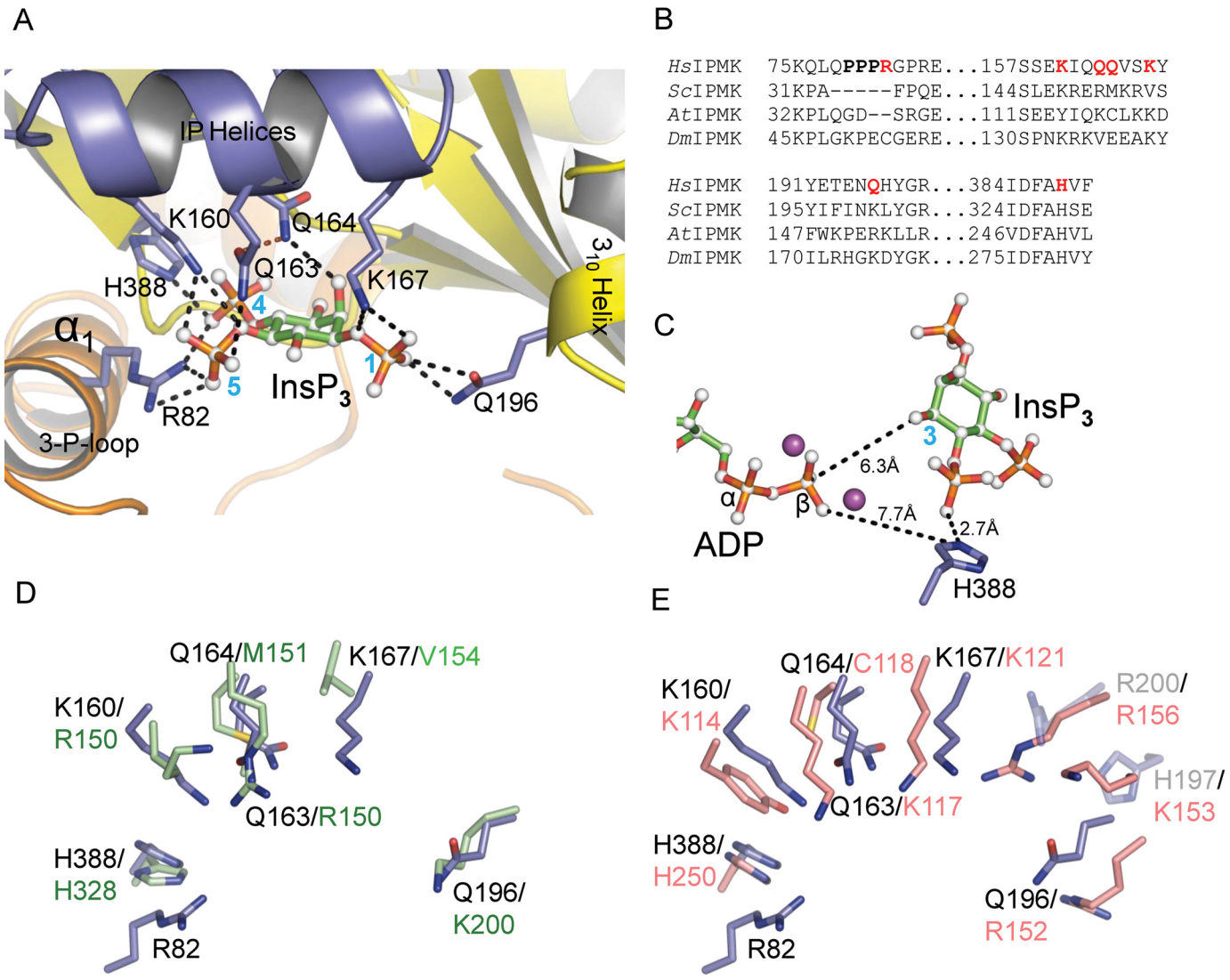

Figure 5. Ins(1,4,5)P_3 binding by IPMKs. *A*, binding of Ins(1,4,5)P_3 within the catalytic site of *Hs*IMPK (stick and ball model; *green stick* for carbon, *red* for oxygen, and *orange* for phosphorus atoms. The phosphate groups are numbered.). *B*, multiple sequence alignment of inositol phosphate-binding regions of IPMKs from the indicated organisms. The tri-Pro sequence is given in *bold*. Residues highlighted in *red* are those involved in binding Ins(1,4,5)P_3 by *Hs*IMPK. *C*, significance of His^{388} in the catalytic center of *Hs*IMPK (stick and ball model; *green stick* for carbon, *red* for oxygen, and *orange* for phosphorus atoms. *D*, superimposition of Ins(1,4,5)P_3-binding residues in *Hs*IPMK (*blue stick*) upon the aligned residues (see *B*) in *Sc*IPMK (*green stick*); *E*, superimposition of Ins(1,4,5)P_3-binding residues in *Hs*IPMK (*blue stick*) upon the aligned residues (see *B*) in *At*IPMK (*pink stick*), plus two additional *At*IPMK residues (Lys^{153} and Arg^{156}, also *pink stick*), which have been implicated in Ins(1,4,5)P_3 binding. The latter two residues align with His^{197} and Arg^{200} in *Hs*IPMK, which do not participate in Ins(1,4,5)P_3 binding; those two *Hs*IPMK residues are shown as a *transparent blue stick*. Note that Arg^{82} in *Hs*IPMK does not have a corresponding residue in either *Sc*IPMK or *At*IPMK.

protein (Fig. 6*C*). These comparisons suggest that, compared with Ins(1,4,5)P_3, IMPK may have a lower binding affinity for Ins(1,3,4,5)P_4; this may be the reason that we were unable to soak Ins(1,3,4,5)P_4 into the active site (see above). Differences in binding affinity may also explain why the rate of Ins(1,3,4,5)P_4 phosphorylation is 90-fold slower than that for Ins(1,4,5)P_3 (Table 2).

We do not exclude the possibility that the orientations of the amino acid side chains might be affected by the nature of the bound substrate. Nevertheless, no such movements were necessary for us to model Ins(1,3,4,5)P_4 into the active site, compared with their positions in the Ins(1,4,5)P_3-bound crystal complex. This situation contrasts with the conclusion that emerged after substrates were modeled into the plant and yeast IPMKs (24, 25). In the latter studies, it was proposed that conformational flexibility was likely an important aspect to accommodating the different substrates within a relatively spacious binding pocket. In those particular IPMK orthologs, such flexibility could be provided by the relatively long and mobile side chains of Lys and Arg (24, 25). In contrast, in the case of *Hs*IPMK, the smaller side chains of Gln have a larger role in substrate-binding.

Mutagenesis of HsIPMK

Elements of the nucleotide-binding domain of *Hs*IMPK are well-conserved within the IP-kinase family (Fig. 2*D*) (21). In contrast, our structural analysis has revealed unique features of the inositol phosphate-binding site, which presumably enforce its own particular set of catalytic activities. We interrogated these new findings using site-directed mutagenesis. We mu-

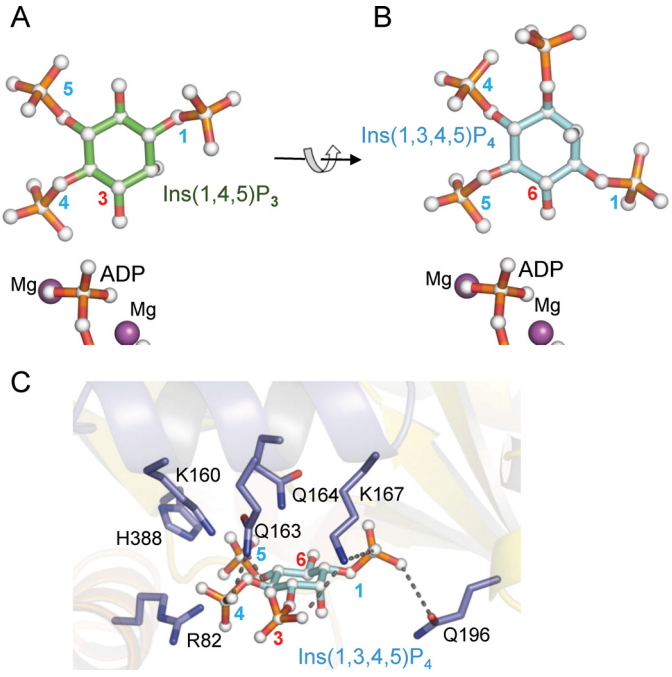

Figure 6. Modeling of Ins(1,3,4,5)P_4 into the substrate-binding pocket of *Hs*IPMK. *A*, the positions of Ins(1,4,5)P_3 (stick and ball model; *green stick* for carbon, *red* for oxygen, and *orange* for phosphorus atoms), magnesium, and ADP within the substrate binding pocket of *Hs*IPMK. *B*, a model for Ins(1,3,4,5)P_4 (stick and ball model; *green stick* for carbon, *red* for oxygen, and *blue* for phosphorus atoms) in the active site, derived by flipping the inositol ring by 180 degrees relative to Ins(1,4,5)P_3. *C*, *dashed lines* depict the proposed interactions between substrate-binding residues and Ins(1,3,4,5)P_4. Carbon groups on the inositol phosphates are numbered.

tated to Ala seven residues that are revealed to interact with Ins(1,4,5)P_3 substrate, together with His^{388} at the catalytic center (Table 2). To varying degrees, each of these mutants exhibited reduced activity compared with wild-type enzyme, for both Ins(1,4,5)P_3 phosphorylation, as well as $InsP_5$ accumulation (Table 2). These mutagenic data validate the conclusions based on structural data (see above) that these particular residues are catalytically important. The H388A mutation had the largest effect, reflecting the critical nature of its role in the catalytic center (Fig. 5*C*).

We also performed a more subtle mutagenic approach to pursue further the particular significance of the three catalytically-important Gln residues at positions 163, 164, and 196: we mutated each to Arg and Lys, both of which have side chains that are larger and also positively charged at physiological pH. The results are quite dramatic (Table 3): in each case, the rate of Ins(1,4,5)P_3 3-kinase activity declined, but in contrast, the rate of Ins(1,3,4,5)P_4 6-kinase activity was not impaired; in fact, three of these mutants showed increased 6-kinase activity (Table 3). From our data on Ins(1,4,5)P_3 binding within the crystal complex (Fig. 5*A*), and our model of Ins(1,3,4,5)P_4 binding (Fig. 6*C*), we can propose 3 possible explanations for why these mutants exhibit a switch in 3-kinase/6-kinase preferences. First, the 3-kinase activity could be impeded by the mutation of Gln^{164} to the larger Lys or Arg residue, because that would provoke a steric conflict with the 2-OH of Ins(1,4,5)P_3, with which Gln^{164} has a favorable interaction in the wild-type enzyme (Fig. 5*A*). For Ins(1,3,4,5)P_4 binding, the 2-OH is rotated out-of-reach from any residue at position 164, because of the ring flip (Fig. 6*C*). Moreover, a gain of function of Ins(1,3,4,5)P_4 6-kinase activity could result from this substrate's 6-OH and 3-phosphate groups making contact with the Lys or Arg replacement (Fig. 6*C*). Second, the relative spatial position of Gln^{164} would be perturbed by mutation of Gln^{163}, because of elimination of the stabilizing electrostatic connection between the two Gln residues (Fig. 5*A*). Third, the substitution of Arg or Lys for Gln^{196} would sterically disturb the latter's favorable interaction with the proximal 1-phosphate of Ins(1,4,5)P_3 (Fig. 5*A*); in the Ins(1,3,4,5)P_4 model, the 1-phosphate is rotated further away from Gln^{196}, but this gap could be bridged by multiple contacts with the larger Lys or Arg, thereby potentially contributing to a 6-kinase gain of function (Fig. 6*C*). These data provide a foundation for the generation and utilization of substrate-selective *Hs*IPMK mutations for a synthetic biology approach to understanding each of the individual biological activities of this multifunctional enzyme.

Structural rationalization of PtdIns(4,5)P_2 3-kinase activity

The determination of the position of the 1-phosphate of Ins(1,4,5)P_3 in the substrate pocket is of particular interest for understanding why PtdIns(4,5)P_2 is also a substrate for *Hs*IMPK. This 1-phosphate, which is doubly ionized (21), makes contacts with both Lys^{167} and Gln^{196} (Fig. 5*A*). In this configuration, a single uncharged oxygen is exposed to the bulk phase; the esterification of this particular oxygen to a diacyclyglycerol backbone would not be expected to impose any steric hindrance to substrate binding. To pursue that idea, we next soaked a soluble diC_4-analogue of PtdIns(4,5)P_2 (along with nucleotide and magnesium) into the *Hs*IMPK apoenzyme crystal; the structure of the enzyme co-complex revealed that the Ins(1,4,5)P_3 headgroup of the inositol lipid was oriented in a near-identical configuration to that of free Ins(1,4,5)P_3 (Fig. 7). Furthermore, three mutations that compromised Ins(1,4,5)P_3 3-kinase activity, Q164A, K167A, and Q196A, had quantitatively similar effects upon PtdIns(4,5)P_2 3-kinase activity (Table 2). These data indicate that there has been co-evolution of Ins(1,4,5)P_3 and PtdIns(4,5)P_2 3-kinase activities.

No electron density was observed for the C_4-diacylglycerol moiety of the PtdIns(4,5)P_2 analogue, indicating that its mobility is not constrained upon binding to *Hs*IPMK. This leaves the natural diacylglycerol backbone free to embed itself either into membranes, or the hydrophobic pockets of certain proteins (14). The position in the crystal complex of the Ins(1,4,5)P_3 headgroup of diC_4-PtdIns(4,5)P_2 clarifies that it can make the same contacts with the protein as Ins(1,4,5)P_3 itself, with just the one exception that the diester phosphate of the lipid at position 1 is held less tightly, because it only carries one negative charge, in contrast to the two in Ins(1,4,5)P_3 (30). Indeed, GroPIns(4,5)P_2 is a 5-fold weaker substrate than Ins(1,4,5)P_3 (Table 2).

Concluding comments

We have described several novel structural features of *Hs*IMPK that clearly distinguish it from the orthologs in *Arabidopsis* and *S. cerevisiae* that predominantly phosphorylate the 6-hydroxyl of Ins(1,4,5)P_3 (24, 25). First, the horseshoe-shaped catalytic site in the human enzyme is more physically constraining. Second, *Hs*IMPK hosts a smaller substrate-binding

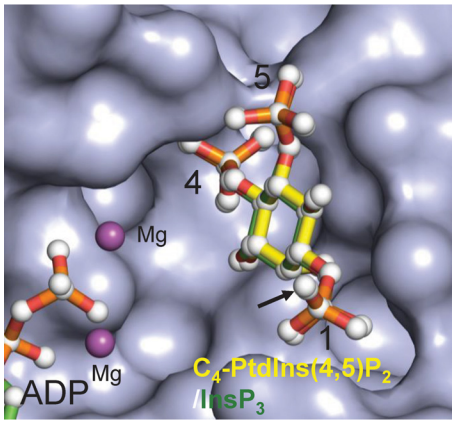

Figure 7. Surface representation of *Hs*IPMK crystal complexes with the Ins(1,4,5)P_3 headgroup of diC_4-PtdIns(4,5)P_2 superimposed upon free Ins(1,4,5)P_3. The figure describes the near-perfectly superimposed (r.m.s. deviation = 0.111 Å) positions of the Ins(1,4,5)P_3 headgroup of diC_4-PtdIns(4,5)P_2 (*yellow* carbon stick) and Ins(1,4,5)P_3 itself (*green* carbon stick). Phosphate groups are numbered. The likely position of the diester attachment is described with a *black arrow*.

pocket in which Gln residues play major roles, unlike the plant and yeast orthologs that are more reliant on the longer and more flexible side chains of Arg and Lys. Third, the proline loop is a unique structural feature of the human enzyme that orients Arg^{82} and Gln^{78} into functionally-important positions within the catalytic pocket. Our results indicate that these are all adaptations that optimize Ins(1,4,5)P_3 phosphorylation predominantly at the 3-position. Our crystal complex data also demonstrate that the Ins(1,4,5)P_3 headgroup of PtdIns(3,4,5)P_3 is near-perfectly superimposed upon free Ins(1,4,5)P_3 itself (Fig. 7). Thus, we propose that 3-kinase positional specificity toward Ins(1,4,5)P_3 has co-evolved along with the functional significance of PtdIns(4,5)P_2 3-kinase activity of *Hs*IPMK. Indeed, *At*IPMK does not express PtdIns(4,5)P_2 3-kinase activity (14, 31), whereas any PtdIns(3,4,5)P_3 product that might be formed in *S. cerevisiae* is not considered to be functional (32). In contrast, the biological importance of the PtdIns(4,5)P_2 3-kinase activity of IMPK in mammals has been well demonstrated (14, 31, 33).

Experimental procedures

Protein expression and purification

The cDNA of *Hs*IPMK was purchased from Addgene (plasmid number 23666). The Gateway expression system (Invitrogen) was used to subclone *Hs*IPMK into the pDest-566 vector. This vector encodes a His_6 tag, a maltose-binding protein tag, and a tobacco etch virus protease cleavage site at the N terminus. Mutants were prepared using a site-directed mutagenesis kit (Stratagene) or a Q5 site-directed mutagenesis kit (Biolabs); all mutants were verified by sequencing. Each pDest-566 vector was used to transform DE3 competent *Escherichia coli* cells (Stratagene) that were pre-transformed with chaperone plasmid pGro7 (Takara, Clontech). An overnight culture of the transformed *E. coli* cells was inoculated into nutrient-rich 2× YT medium supplemented with 0.07% (w/v) L-arabionose at pH 7.5 and grown at 37 °C to A595 = 0.7. Isopropyl β-D-thiogalactopyranoside (0.1 mM) was then added and cultures were continued at 15 °C for 20 h. The cells were disrupted using a constant cell disruption system (Constant Systems LTD) under 20 KPsi. Recombinant wild-type and mutant proteins were purified by several chromatographic procedures performed at 4 °C. First, the protein was applied to a nickel-nitrilotriacetic acid-agarose column (Qiagen), washed with buffer containing 300 mM NaCl, 20 mM Tris-HCl, pH 7.5, 20 mM imidazole, then eluted by increasing the imidazole concentration to 400 mM. Second, the eluate was applied to a HiTrap™ Heparin HP column (GE Healthcare) and eluted with 10 column volumes of a 50–2000 mM NaCl gradient in 20 mM Tris-HCl (pH 7.5). Next, after tobacco etch virus protease cleavage, the protein was further purified using another HiTrap™ Heparin HP column, and finally, a Superdex™ 200 gel filtration column (GE Healthcare) that was eluted with 150 mM NaCl, 20 mM Tris-HCl, pH 7.5. Purified proteins were concentrated to either 0.5–2 mg/ml (for assaying catalytic activities) or 30 mg/ml (for crystallization); storage was at −80 °C.

Crystallization

The core catalytic domain of *Hs*IPMK (residues: $^{50-262}$Gly-Gly-Ser-Gly-Gly$^{378-416}$; Fig. 2*A*) was initially screened for optimum crystallization conditions using the mosquito-LCP (TTP Labtech). Multiple conditions that each contained a high concentration of PEG 400 were identified. Final conditions were optimized by hanging drop vapor diffusion, against a well buffer of 35% (w/v) PEG 400, 0.1 M Li_2SO_4, 100 mM MES-imidazole buffer, pH 6.0, 50 mM β-mercaptoethanol at 25 °C (2 μl of 38 mg/ml of protein plus 2 μl of well buffer in the crystallization drop). To obtain complex structures, apoenzyme crystals were further soaked for 1 day in 35% (w/v) PEG 400, 100 mM Li_2SO_4, 100 mM HEPES, pH 7.5, at 25 °C, in the presence of 20 mM Ins(1,4,5)P_3 or a soluble diC_4-analogue of PtdIns(4,5)P_2, 10 mM $MgCl_2$, and 5 mM of either Na_2ATP or Li_2AMP-PNP; mother liquid was used for cryoprotection. The same conditions were used in attempts to soak Ins(1,3,4,5)P_4 into the crystals, in the presence of either ATP or ADP, but we were unable to define any clear electron density for the inositol phosphate.

Data collection, structure determination, and refinement

Diffraction data were collected using APS beamlines 22-ID and 22-BM. All data were processed with the program HKL2000 (34). Initial phases for the structure were determined by molecular replacement with the autoMR program in the CCP4 package (35, 36), using *Sc*IPMK structure (PDB code 2IF8; sequence identity 31%) as a search model. This initial structure was manually rebuilt with COOT and refined with REFMAC from the CCP4 package. The other crystal structures were determined by using rigid body and direct Fourier synthesis, and refined with the equivalent and expanded test sets. The molecular graphics representations were prepared with the program PyMol (Schrödinger, LLC). Atomic coordinates and structure factors have been deposited with the Protein Data Bank with accession codes 5W2G, 5W2H, and 5W2I.

Enzyme assays and HPLC analysis

We used HPLC (37) to analyze the catalytic activities of *Hs*IPMK toward [^{3}H]Ins(1,4,5)P_3 (American Radiolabeled Chemicals). In these reactions, *Hs*IPMK sequentially phos-

phorylates Ins(1,4,5)P_3 to Ins(1,3,4,5)P_4 to Ins(1,3,4,5,6)P_5 (see "Results and Discussions" and Ref. 11). We circumvented the problem that [^{3}H]Ins(1,3,4,5)P_4 is not commercially available, by generating first-order rate constants for the two sequential reactions (38), from time-dependent changes in levels of Ins(1,4,5)P_3, Ins(1,3,4,5)P_4, and Ins(1,3,4,5,6)P_5. We assayed the PtdIns(4,5)P_2 3-kinase activity of *Hs*IPMK by using soluble GroPtd[^{3}H]Ins(4,5)P_2 (prepared by deacylation (39) of Ptd[^{3}H]Ins(4,5)P_2 (American Radiolabeled Chemicals)).

Kinase assays were performed by incubating either wild-type *Hs*IPMK or mutants with trace quantities of either [^{3}H]Ins(1,4,5)P_3 or GroPtd[^{3}H]Ins(4,5)P_2 at 37 °C, in 100 μl of buffer containing 1 mM EDTA, 100 mM KCl, 20 mM HEPES, pH 7.2, 8 mM $MgSO_4$, 5 mM Na_2ATP. All reactions were acid quenched (0.2 volumes of 2 M perchloric acid + 1 mg/ml of $InsP_6$), and neutralized (40). For some experiments, assays contained 1 mM EDTA, 100 mM KCl, 20 mM HEPES, pH 7.2, 3 mM $MgSO_4$, 100 μM diC$_8$-PtdIns(4,5)P_2 (Cellsignals), 50 μM Na_2ATP plus 50,000 dpm of [^{32}P]ATP (MP Biomedicals); prior to HPLC analysis, the diC$_8$-Ptd[^{32}P]Ins(3,4,5)P_3 product was deacylated (39).

All assays were analyzed by ion-exchange HPLC, using an Adsorbosphere Q100 column. The elution gradient was generated by mixing Buffer A (1 mM Na_2EDTA) with Buffer B (Buffer A plus 2 M $NH_4H_2PO_4$, pH 3.9, with H_3PO_4) as follows: 0–5 min, 0% B; 5–10 min, 0–16% B, 10–60 min, 16–36% B, 60–61 min, 36–70% B. Radioactivity was measured either with an in-line counter using UltimaFlo AP (PerkinElmer Life Sciences), or by collecting 1-ml fractions, which were mixed with MonoFlow-4 (National Diagnostics); in all experiments, data are plotted as % of total radioactivity shown (in cpm or dpm).

Standards of both [^{14}C]Ins(1,4,5,6)P_4 and [^{14}C]Ins(1,3,4,5,6)P_5 were prepared as described previously (41). A standard of GroPtd[^{32}P]Ins(3,4,5)P_3 was prepared by deacylation (39) of Ptd[^{32}P]Ins(3,4,5)P_3 produced as follows: 50 ng of PIK3CA and PtdIns(4,5)P_2 (both supplied in a PI3K assay kit, product number 17–493, Millipore) were incubated at 37 °C for 16 h in 100 μl of buffer containing 1 mM EDTA, 100 mM KCl, 20 mM HEPES, pH 7.2, 3 mM $MgSO_4$, 50 μM Na_2ATP plus 50,000 dpm of [^{32}P]ATP (MP Biomedicals).

Author contributions—H. W. performed all of the experiments and analyzed the results. H. W. conceived and designed the experiments. H. W. and S. B. S. wrote the paper.

Acknowledgments—We thank Traci M. T. Hall and Chen Qiu for critical reading of the manuscript and the NIEHS Collaborative crystallography group, the Advanced Photon Source (APS) SE Regional Collaborative Access Team (SER-CAT) 22-ID and 22-BM beam lines for assistance with crystallographic data collection.

References

1. Shears, S. B. (2017) Intimate connections: inositol pyrophosphates at the interface of metabolic regulation and cell signaling. *J. Cell Physiol.* 10.1002/jcp.26017
2. Odom, A. R., Stahlberg, A., Wente, S. R., and York, J. D. (2000) A role for nuclear inositol 1,4,5-trisphosphate kinase in transcriptional control. *Science* **287,** 2026–2029
3. Saiardi, A., Erdjument-Bromage, H., Snowman, A. M., Tempst, P., and Snyder, S. H. (1999) Synthesis of diphosphoinositol pentakisphosphate by a newly identified family of higher inositol polyphosphate kinases. *Curr. Biol.* **9,** 1323–1326
4. Resnick, A. C., Snowman, A. M., Kang, B. N., Hurt, K. J., Snyder, S. H., and Saiardi, A. (2005) Inositol polyphosphate multikinase is a nuclear PI3-kinase with transcriptional regulatory activity. *Proc. Natl. Acad. Sci. U.S.A.* **102,** 12783–12788
5. Frederick, J. P., Mattiske, D., Wofford, J. A., Megosh, L. C., Drake, L. Y., Chiou, S. T., Hogan, B. L., and York, J. D. (2005) An essential role for an inositol polyphosphate multikinase, *Ipk2,* in mouse embryogenesis and second messenger production. *Proc. Natl. Acad. Sci. U.S.A.* **102,** 8454–8459
6. Leyman, A., Pouillon, V., Bostan, A., Schurmans, S., Erneux, C., and Pesesse, X. (2007) The absence of expression of the three isoenzymes of the inositol 1,4,5-trisphosphate 3-kinase does not prevent the formation of inositol pentakisphosphate and hexakisphosphate in mouse embryonic fibroblasts. *Cell Signal.* **19,** 1497–1504
7. Fujii, M., and York, J. D. (2005) A role for rat inositol polyphosphate kinases, rIpk2 and rIpk1, in inositol pentakisphosphate and inositol hexakisphosphate production in Rat-1 cells. *J. Biol. Chem.* **280,** 1156–1164
8. Barker, C. J., and Berggren, P.-O. (1999) Inositol hexakisphosphate and b-cell stimulus-scretion coupling. *Anticancer Res.* **19,** 3737–3741
9. Gao, Y., and Wang, H. Y. (2007) Inositol pentakisphosphate mediates Wnt/β-catenin signaling. *J. Biol. Chem.* **282,** 26490–26502
10. El Bakkoury, M., Dubois, E., and Messenguy, F. (2000) Recruitment of the yeast MADS-box proteins, ArgRI and Mcm1 by the pleitropic factor ArgRIII is required for their stability. *Mol. Microbiol.* **35,** 15–31
11. Nalaskowski, M. M., Deschermeier, C., Fanick, W., and Mayr, G. W. (2002) The human homologue of yeast ArgRIII protein is an inositol phosphate multikinase with predominantly nuclear localization. *Biochem. J.* **366,** 549–556
12. Ramazzotti, G., Faenza, I., Fiume, R., Billi, A. M., Manzoli, L., Mongiorgi, S., Ratti, S., McCubrey, J. A., Suh, P. G., Cocco, L., and Follo, M. Y. (2017) PLC-β1 and cell differentiation: an insight into myogenesis and osteogenesis. *Adv. Biol. Regul.* **63,** 1–5
13. Wickramasinghe, V. O., Savill, J. M., Chavali, S., Jonsdottir, A. B., Rajendra, E., Grüner, T., Laskey, R. A., Babu, M. M., and Venkitaraman, A. R. (2013) Human inositol polyphosphate multikinase regulates transcript-selective nuclear mRNA export to preserve genome integrity. *Mol. Cell* **51,** 737–750
14. Blind, R. D., Suzawa, M., and Ingraham, H. A. (2012) Direct modification and activation of a nuclear receptor-PIP2 complex by the inositol lipid kinase IPMK. *Sci. Signal.* **5,** ra44
15. Kim, S., Kim, S. F., Maag, D., Maxwell, M. J., Resnick, A. C., Juluri, K. R., Chakraborty, A., Koldobskiy, M. A., Cha, S. H., Barrow, R., Snowman, A. M., and Snyder, S. H. (2011) Amino acid signaling to mTOR mediated by inositol polyphosphate multikinase. *Cell Metab.* **13,** 215–221
16. Xu, R., Sen, N., Paul, B. D., Snowman, A. M., Rao, F., Vandiver, M. S., Xu, J., and Snyder, S. H. (2013) Inositol polyphosphate multikinase is a coactivator of p53-mediated transcription and cell death. *Sci. Signal.* **6,** ra22
17. Bang, S., Kim, S., Dailey, M. J., Chen, Y., Moran, T. H., Snyder, S. H., and Kim, S. F. (2012) AMP-activated protein kinase is physiologically regulated by inositol polyphosphate multikinase. *Proc. Natl. Acad. Sci. U.S.A.* **109,** 616–620
18. Sei, Y., Zhao, X., Forbes, J., Szymczak, S., Li, Q., Trivedi, A., Voellinger, M., Joy, G., Feng, J., Whatley, M., Jones, M. S., Harper, U. L., Marx, S. J., Venkatesan, A. M., Chandrasekharappa, S. C., *et al.* (2015) A hereditary form of small intestinal carcinoid associated with a germline mutation in inositol polyphosphate multikinase. *Gastroenterology* **149,** 67–78
19. Ahmed, I., Sbodio, J. I., Harraz, M. M., Tyagi, R., Grima, J. C., Albacarys, L. K., Hubbi, M. E., Xu, R., Kim, S., Paul, B. D., and Snyder, S. H. (2015) Huntington's disease: Neural dysfunction linked to inositol polyphosphate multikinase. *Proc. Natl. Acad. Sci. U.S.A.* **112,** 9751–9756
20. Yokoyama, J. S., Wang, Y., Schork, A. J., Thompson, W. K., Karch, C. M., Cruchaga, C., McEvoy, L. K., Witoelar, A., Chen, C. H., Holland, D., Brewer, J. B., Franke, A., Dillon, W. P., Wilson, D. M., Mukherjee, P., *et al.*

(2016) Association between genetic traits for immune-mediated diseases and Alzheimer disease. *JAMA Neurol.* **73,** 691–697
21. González, B., Schell, M. J., Letcher, A. J., Veprintsev, D. B., Irvine, R. F., and Williams, R. L. (2004) Structure of a human inositol 1,4,5-trisphosphate 3-kinase; substrate binding reveals why it is not a phosphoinositide 3-kinase. *Mol. Cell* **15,** 689–701
22. Miller, G. J., and Hurley, J. H. (2004) Crystal structure of the catalytic core of inositol 1,4,5-trisphosphate 3-kinase. *Mol. Cell* **15,** 703–711
23. Wang, H., DeRose, E. F., London, R. E., and Shears, S. B. (2014) IP6K structure and the molecular determinants of catalytic specificity in an inositol phosphate kinase family. *Nat. Commun.* **5,** 4178
24. Holmes, W., and Jogl, G. (2006) Crystal structure of inositol phosphate multikinase 2 and implications for substrate specificity. *J. Biol. Chem.* **281,** 38109–38116
25. Endo-Streeter, S., Tsui, M. K., Odom, A. R., Block, J., and York, J. D. (2012) Structural studies and protein engineering of inositol phosphate multikinase. *J. Biol. Chem.* **287,** 35360–35369
26. Meyer, R., Nalaskowski, M. M., Ehm, P., Schröder, C., Naj, X., Brehm, M. A., and Mayr, G. W. (2012) Nucleocytoplasmic shuttling of human inositol phosphate multikinase is influenced by CK2 phosphorylation. *Biol. Chem.* **393,** 149–160
27. Madhusudan, Akamine, P., Xuong, N. H., and Taylor, S. S. (2002) Crystal structure of a transition state mimic of the catalytic subunit of cAMP-dependent protein kinase. *Nat. Struct. Biol.* **9,** 273–277
28. Stout, T. J., Foster, P. G., and Matthews, D. J. (2004) High-throughput structural biology in drug discovery: protein kinases. *Curr. Pharm. Des.* **10,** 1069–1082
29. Cheek, S., Ginalski, K., Zhang, H., and Grishin, N. V. (2005) A comprehensive update of the sequence and structure classification of kinases. *BMC Struct. Biol.* **5,** 6
30. Kooijman, E. E., King, K. E., Gangoda, M., and Gericke, A. (2009) Ionization properties of phosphatidylinositol polyphosphates in mixed model membranes. *Biochemistry* **48,** 9360–9371
31. Maag, D., Maxwell, M. J., Hardesty, D. A., Boucher, K. L., Choudhari, N., Hanno, A. G., Ma, J. F., Snowman, A. S., Pietropaoli, J. W., Xu, R., Storm, P. B., Saiardi, A., Snyder, S. H., and Resnick, A. C. (2011) Inositol polyphosphate multikinase is a physiologic PI3-kinase that activates Akt/PKB. *Proc. Natl. Acad. Sci. U.S.A.* **108,** 1391–1396
32. Rodríguez-Escudero, I., Roelants, F. M., Thorner, J., Nombela, C., Molina, M., and Cid, V. J. (2005) Reconstitution of the mammalian PI3K/PTEN/Akt pathway in yeast. *Biochem. J.* **390,** 613–623
33. Kim, E., Beon, J., Lee, S., Park, J., and Kim, S. (2016) IPMK: A versatile regulator of nuclear signaling events. *Adv. Biol. Regul.* **61,** 25–32
34. Otwinowski, Z., and Minor, W. (1997) Processing of X-ray diffraction data collected in oscillation mode. *Methods Enzymol.* **276,** 307–326
35. Emsley, P., and Cowtan, K. (2004) Coot: model-building tools for molecular graphics. *Acta Crystallogr. D Biol. Crystallogr.* **60,** 2126–2132
36. Winn, M. D., Murshudov, G. N., and Papiz, M. Z. (2003) Macromolecular TLS refinement in REFMAC at moderate resolutions. *Methods Enzymol.* **374,** 300–321
37. Stevenson-Paulik, J., Chiou, S. T., Frederick, J. P., dela Cruz, J., Seeds, A. M., Otto, J. C., and York, J. D. (2006) Inositol phosphate metabolomics: merging genetic perturbation with modernized radiolabeling methods. *Methods* **39,** 112–121
38. Davies, D. D. (1961) Intermediary Metabolism in Plants, Cambridge University Press, Cambridge, United Kingdom
39. Shears, S. B. (1997) Measurement of inositol phosphate turnover in intact cells and cell-free systems. in Signalling by Inositides: a Practical Approach (Shears, S. B., ed) pp. 33–52, Oxford University Press, Oxford, UK
40. Gu, C., Nguyen, H. N., Hofer, A., Jessen, H. J., Dai, X., Wang, H., and Shears, S. B. (2017) The significance of the bifunctional kinase/phosphatase activities of PPIP5Ks for coupling inositol pyrophosphate cell-signaling to cellular phosphate homeostasis. *J. Biol. Chem.* **292,** 4544–4555
41. Craxton, A., Erneux, C., and Shears, S. B. (1994) Inositol 1,4,5,6-tetrakisphosphate is phosphorylated in rat liver by a 3-kinase that is distinct from inositol 1,4,5-trisphosphate 3-kinase. *J. Biol. Chem.* **269,** 4337–4342